Supplemental Information

Structure of the human UBR5 E3 ubiquitin ligase

Feng Wang, Qing He, Wenhu Zhan, Ziqi Yu, Efrat Finkin-Groner, Xiaojing Ma, Gang Lin, Huilin Li
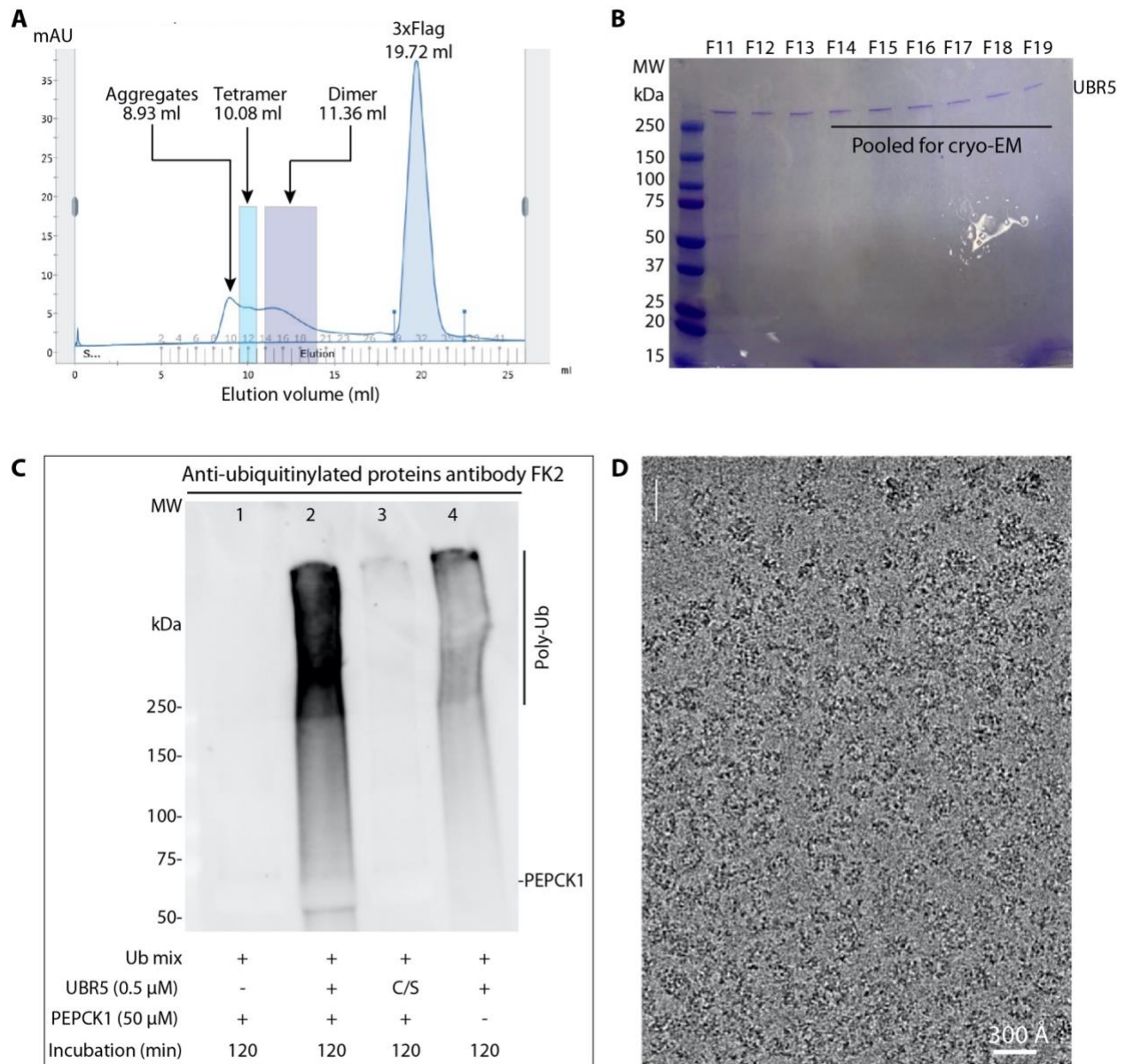
Figure S1. Purification and characterization of UBR5, related to Figure 1 and 2.

(**A**) Size exclusion chromatogram of insect expressed human UBR5 using a Superose 6 column (10/300 GL, GE Healthcare). The elution volumes of the two marked peaks are consistent with UBR5 dimer and tetramer. (**B**) SDS-PAGE gel of fractions 11 to 19 of the gel filtration profile. Fractions 14 to 19 were pooled for activity assay and cryo-EM analysis. (**C**) Western blot analysis of in vitro ubiquitylation reaction of the WT and the catalytically dead (C2768S, C/S) UBR5 using purified PEPCK1 as an acceptor substrate. The input amounts of UBR5 and UBR5 mutants were first normalized by performing SDS-PAGE gel before the assay. The samples contained both dimer and tetramer. The FK2 multiubiquitin chain monoclonal antibody was used for blotting. The Ub mix contained Ub, E1, and E2D2. (**D**) A typical raw electron micrograph of the purified WT UBR5 particles embedded in vitreous ice.
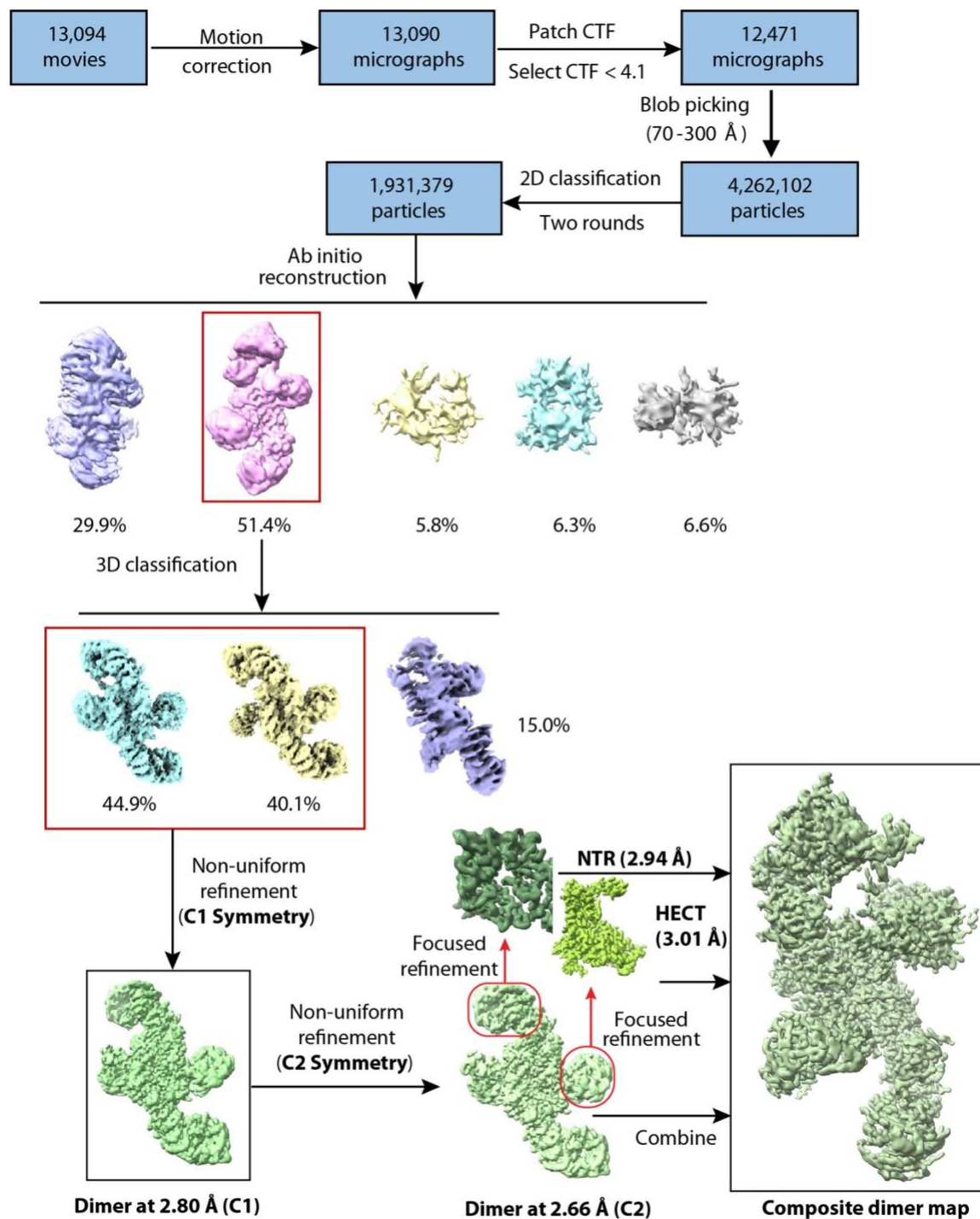
Figure S2. Workflow of cryo-EM data processing and 3D reconstruction of UBR5 homodimer, related to Figure 1.

CryoSPARC (version 3.2.0) is used for image processing and 3D reconstruction, yielding the 2.8-Å resolution 3D map in the C1 symmetry and the 2.66-Å resolution 3D map in the C2 symmetry. Focused refinement of the C2 map improved the NTR (including β-propeller domain and SBB1) and HECT domain. The NTR and HECT maps were combined with the C2 symmetry map to obtain the composite map in ChimeraX.
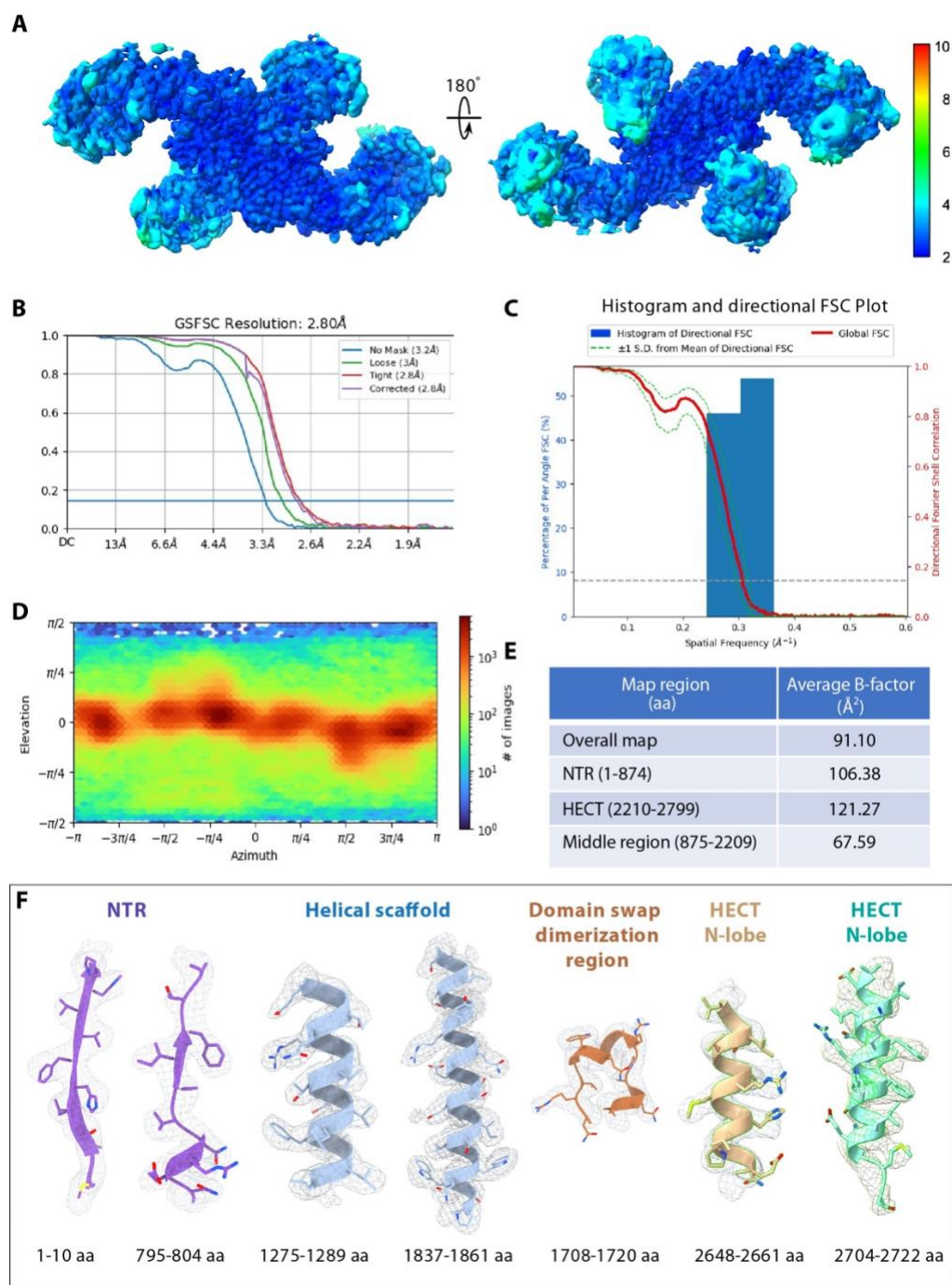
Figure S3. Resolution estimation of the 3D map of UBR5 homodimer, related to Figure 1 and 2.
(**A**) Color coded local resolution map of the UBR5 dimer EM map. (**B**) The gold standard Fourier shell correlation curves of the final 3D map. (**C**) The directional anisotropy of the UBR5 3D map as quantified by the 3D-FSC server (https://3dfsc.salk.edu/). The 3D map has a good anisotropic property with a sphericity of 0.962. (**D**) Angular distribution of particle images used in the final reconstruction. (**E**) Average B factors for whole map and individual regions. (**F**) Fit between the EM map and the model in seven selected regions.
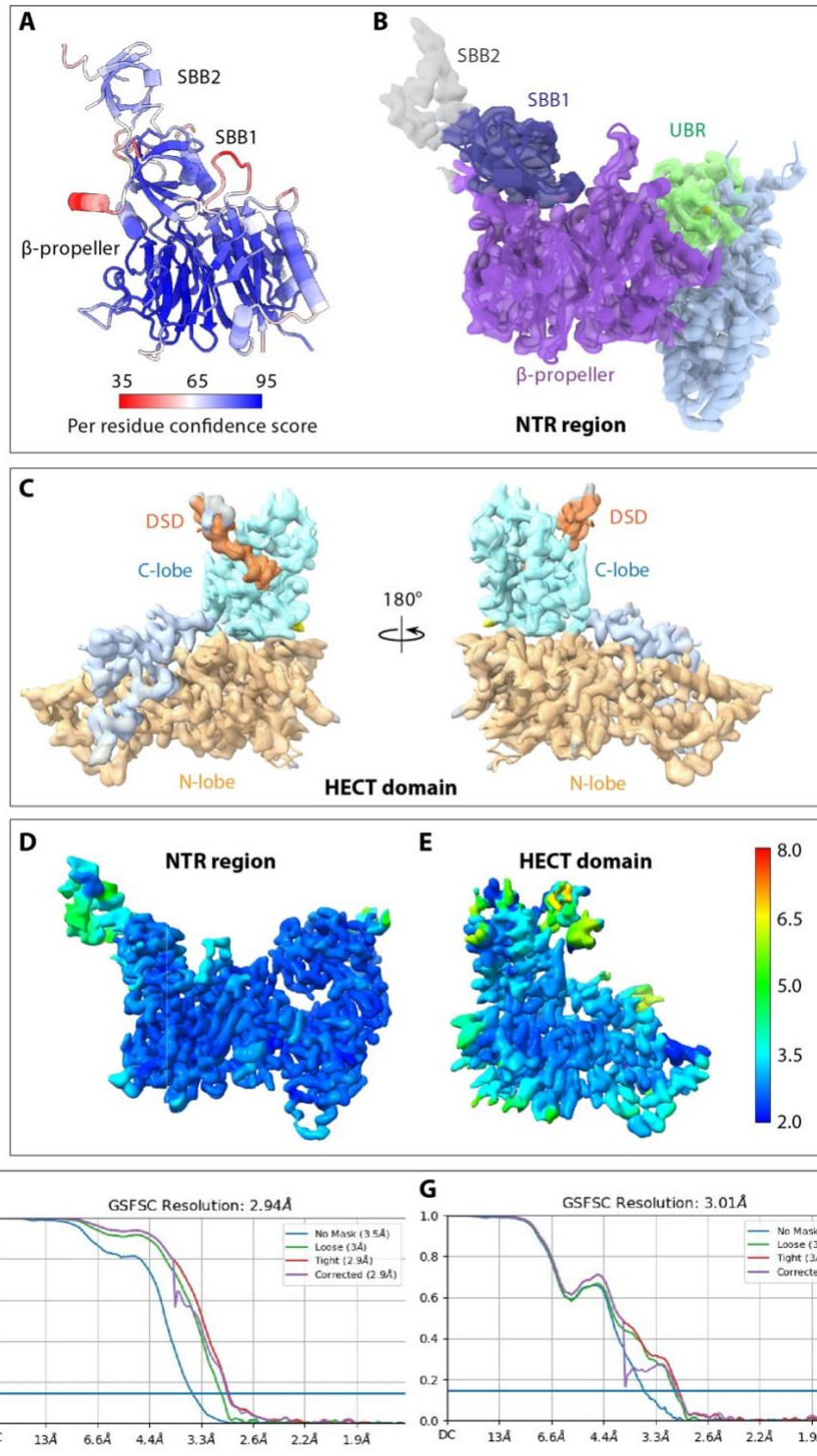
Figure S4. Focus-refined maps of the UBR5 NTR and HECT, related to Figure 2 and 3.
(**A**) AlphaFold2 predicted structure of NTR, colored by the per-residue confidence score. Both SBB1 and β-propeller have high confidence score. (**B**) Focus-refined NTR EM map. Many β strands in the β-propeller and SBB1 are resolved. The SBB2 density (gray) is too weak to model. (**C**) Focus-refined HECT EM map. (**D-E**) The focus-refined NTR (d) and HECT EM maps color coded by local resolution. (**F-G**) The gold-standard Fourier shell correlation (GSFSC) curves of the final focused on refinement 3D maps of the NTR and HECT, respectively.
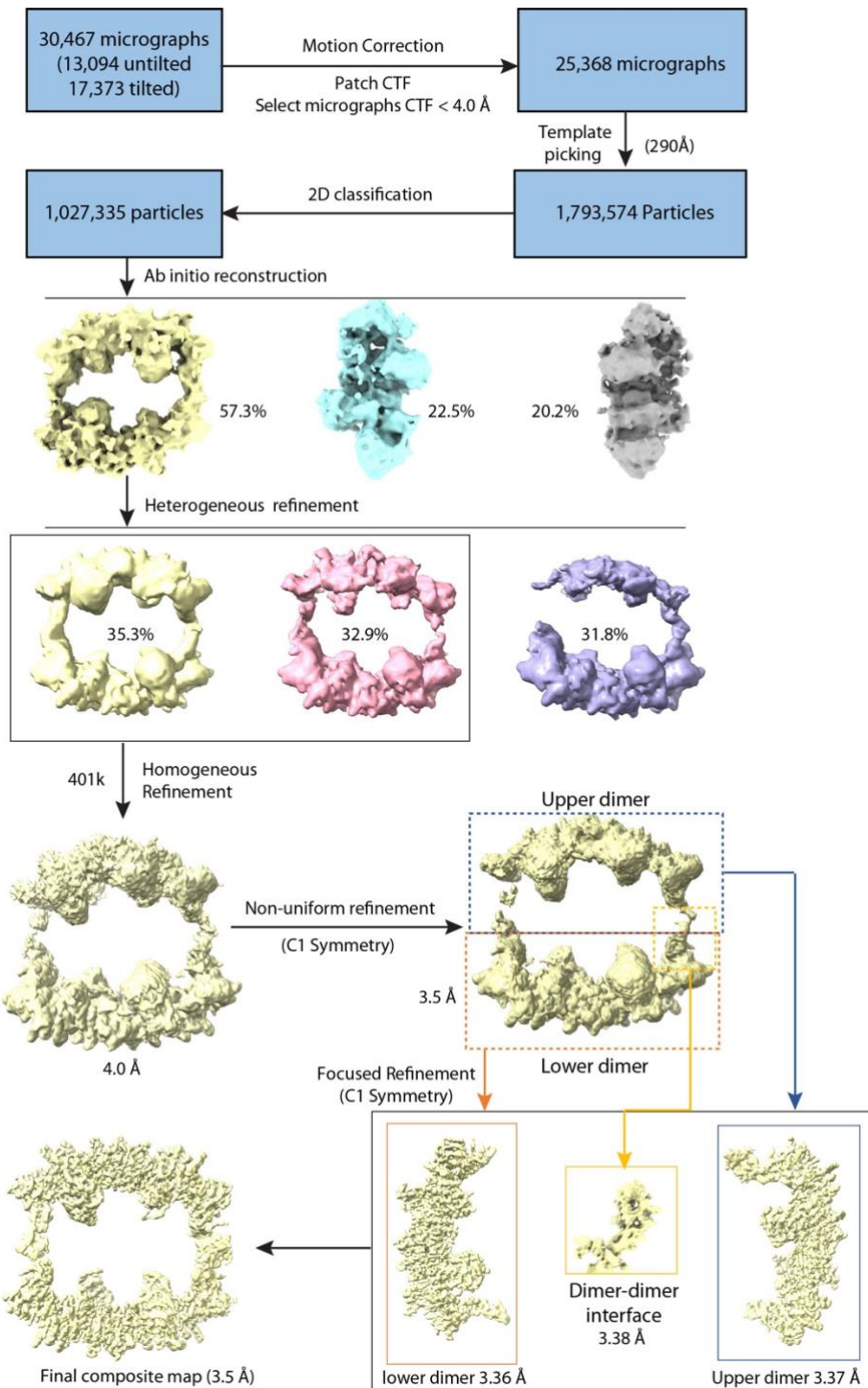
Figure S5. Workflow of cryo-EM data processing and 3D reconstruction of UBR5 tetramer, related to Figure 1 and 4.
CryoSPARC (version 3.2.0) is used for processing the untilted and titled datasets. The non-uniform refined 3D map of the tetramer was at 3.5 Å resolution in C1 symmetry. Focused refinement on the upper and lower dimers and the dimer-dimer interface region led to slightly improved local maps. These maps were combined in ChimeraX to obtain the final composite tetramer map at ~3.5 Å resolution.
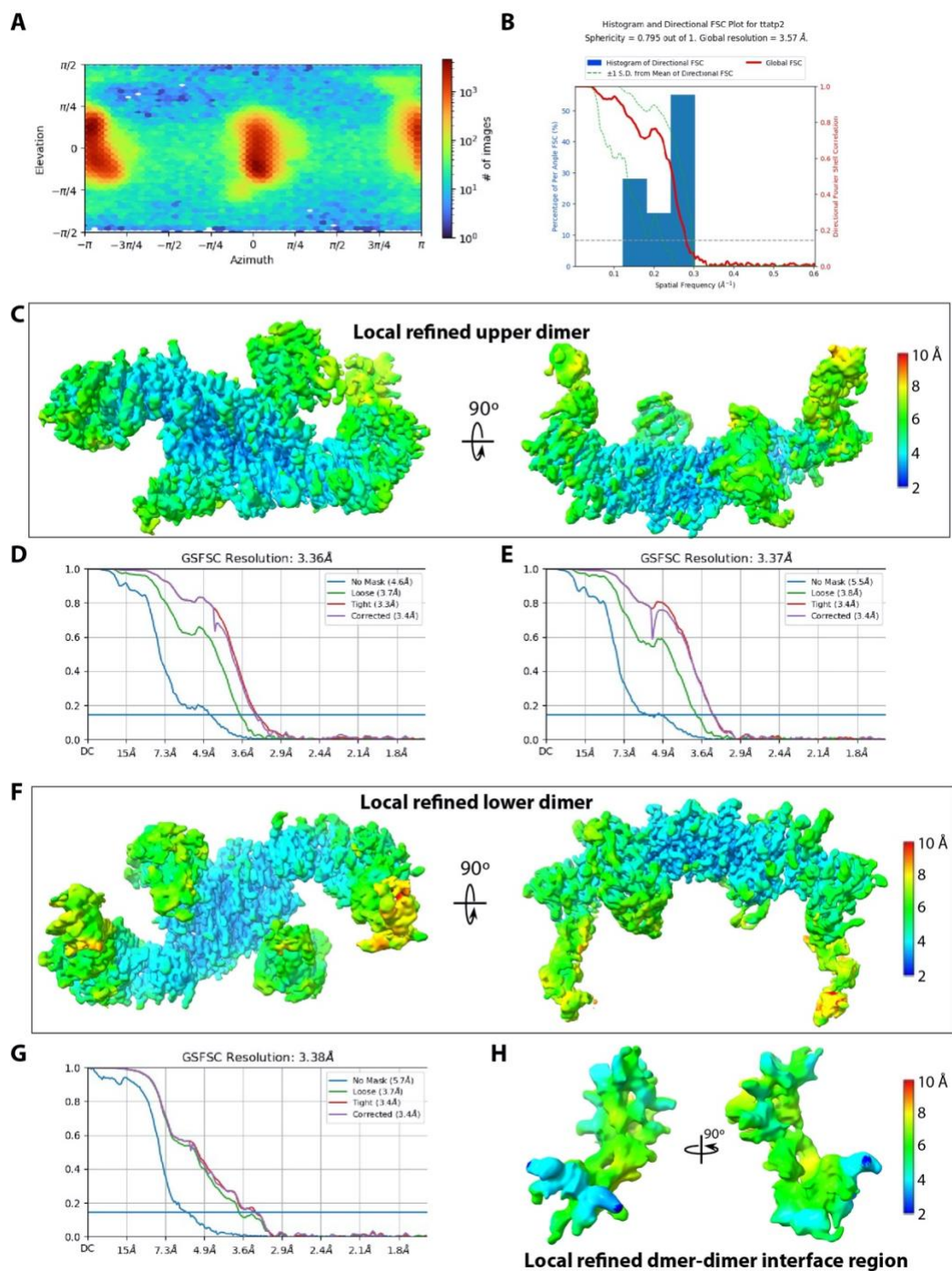
Figure S6. Resolution estimation of the focus refined EM maps of the UBR5 tetramer, related to Figure 1 and 4.
(**A**) Angular distribution of tetramer particle images used in the final reconstruction. (**B**) Histogram and directional FSC Plot of the 3D map as quantified by the 3D-FSC server (https://3dfsc.salk.edu/). (**C**) Focus-refined upper dimer map color coded by local resolution. (**D-E**) The gold standard Fourier shell correlation curves of the upper and lower focus-refined UBR5 dimer maps. (**F**) Focus-refined lower dimer map color coded by local resolution. (**G**) The gold standard Fourier shell correlation curves of the focus-refined dimer-dimer interface region map. (**H**) Focus-refined the interface region map color coded by local resolution.
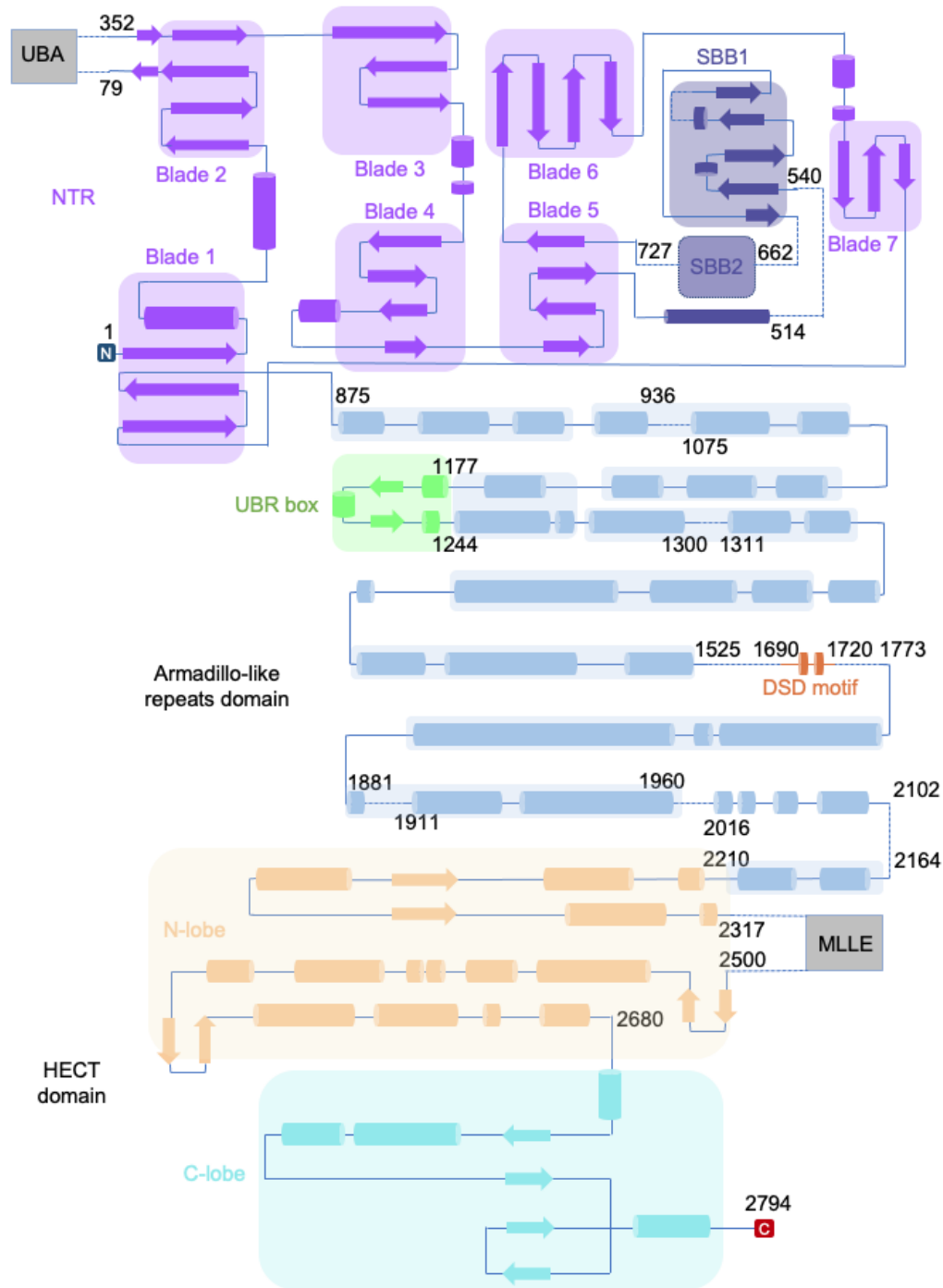
Figure S7. Topological diagram of UBR5, related to Figure 1.
The α-helices are represented by cylinders and β-strands by thick arrows. The regions and domains are colored as in Fig.1a. The resolved domains (UBA, SBB2, and MLLE) and unstructured regions are shown as dark rectangles and dashed lines, respectively. The structured regions account for >60% of the sequence.
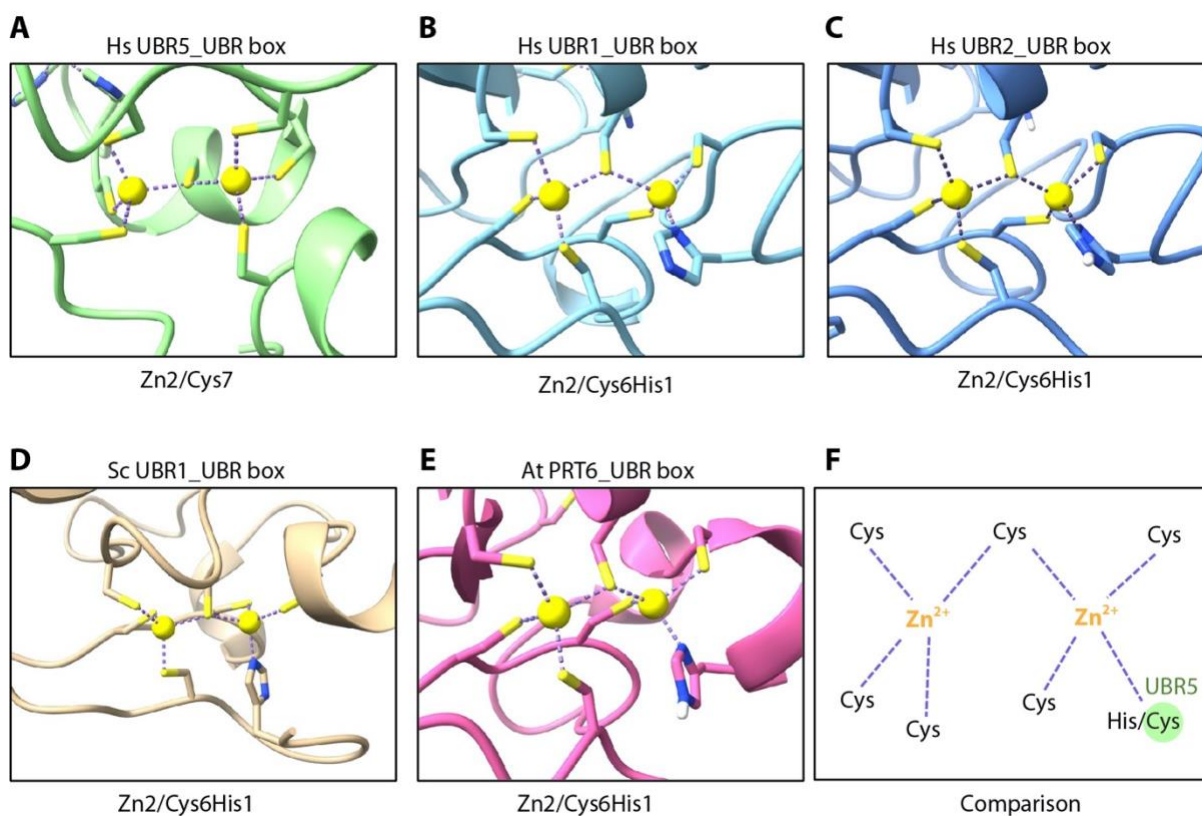
Figure S8. Close-up views of the two Zinc coordination in the UBR5 UBR box and other proteins, related to Figure 3.

(**A**) The Zn2/Cys7 coordination style from HsUBR5_UBR box (PDB ID 8D4X). (**B-C**) The Zn2/Cys6His1 coordination style from HsUBR1_UBR box (PDB ID 3NY2) and HsUBR2_UBR box (PDB ID 5TDA). (**D**) The Zn2/Cys6His1 coordination style from Sc UBR1_UBR box (PDB ID 3NIS). (**E**) The Zn2/Cys6His1 coordination style from At PRT6_UBR box (PDB ID 6LHN). (**F**) Schematic of the two Zinc coordination in the UBR box, showing that only UBR5 substitutes His with Cys in the general Zn2/Cys6His1 coordination.
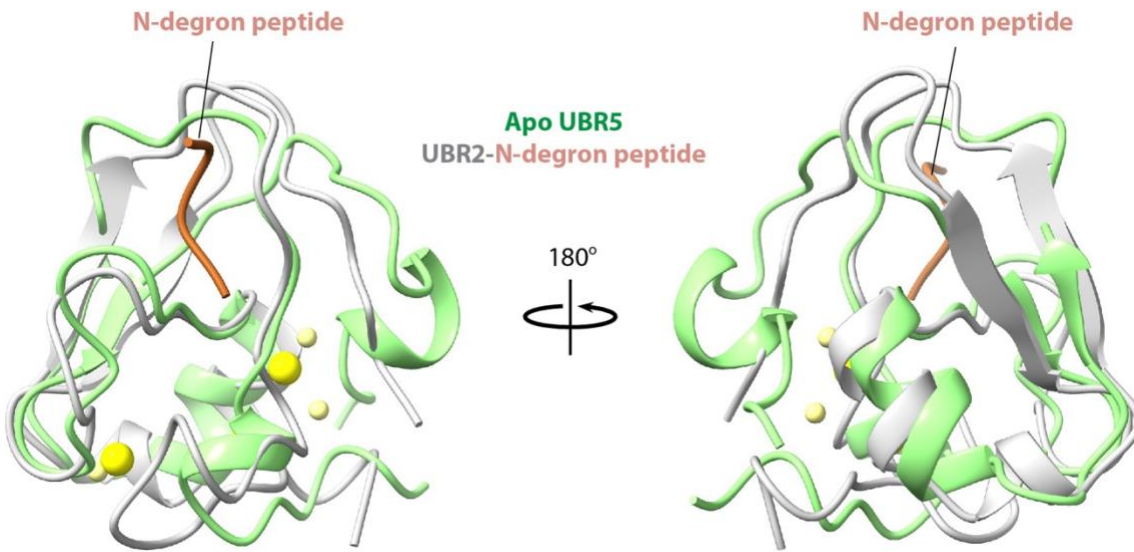
Figure S9. Superimposition of the UBR5 UBR-box and the N-degron peptide bound UBR2 UBR-box, related to Figure 3.
The two structures of Apo UBR5 and UBR2 with N-degron peptide aligned well with an RMSD of 1.8 Å.
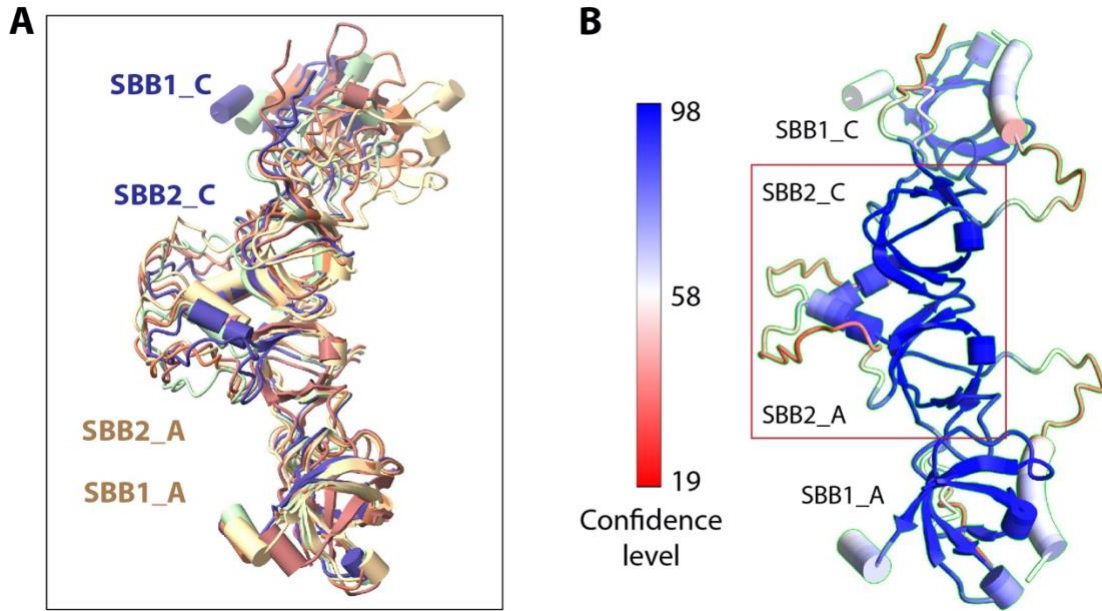
Figure S10. The predicted SBB-SBB2 dimer structure at the UBR5 tetramer interface, related to Figure 4.

(**A**) Superposition of the top five [SBB1-SBB2]$_2$ dimer structural models predicted by the AlphaFold-multimer. Each model was shown in a different color. (**B**) The atomic model of SBB1-2 dimer was colored by the per-residue confidence score. The interface of SBB2-SBB2 in the orange square has high confidence score.

Table S1. **Cryo-EM data collection, refinement, and validation statistics, related to Figure 1 and 2.**

	UBR5 dimer (EMDB-27201, PDB 8D4X)	UBR5 dimer (EMDB-27822, PDB 8E0Q)	UBR5 tetramer (EMDB-28646, PDB 8EWI)
Data collection and processing			
Microscope	FEI Titan Krios		FEI Titan Krios
Magnification	105,000		105,000
Voltage (kV)	300		300
Electron exposure (e–/Å^2/sec)	43.8		43.8
Defocus range (μm)	−1.0 to −2.0		−1.0 to −2.0
Focus step (μm)	0.2		0.2
Pixel size (Å/pixel)	0.828		0.828
Initial particle images (no.)	4,262,102		1,793,574(1,245,550 untilted + 548,024 tilted)
Final particle images (no.)	844,403		401,468(310,245 untilted + 91,223 tilted)
Symmetry imposed	C1	C2	C1
Map resolution (Å)	2.80	2.66	3.38
FSC threshold	0.143	0.143	0.143
Refinement			
Model resolution (Å)	3.1	3.1	4.0
FSC threshold	0.5	0.5	0.5
Model resolution range (Å)	1.8-5.3	1.8-6.2	2.2-8.0
Map sharpening B factor (Å^2)	118.3	119	104.4
Model composition			
Non-hydrogen atoms	26409	26604	55708
Protein residues	3353	3378	7100
Ligands	6	6	12
B factors (Å^2)			
Protein mean (min/max)	91.10 (9.51/193.28)	81.19 (17.94/193.48)	122.93 (58.90/251.96)
Ligand mean (min/max)	90.28 (63.81/128.74)	82.69 (66.95/96.58)	104.76 (75.01/127.73)
R.m.s. deviations			
Bond lengths (Å)	0.003	0.003	0.002
Bond angles (°)	0.693	0.519	0.539
Validation			
MolProbity score	2.21	2.33	2.41
Clashscore	12.82	9.95	12.88
Poor rotamers (%)	2.44	4.74	3.94
Ramachandran plot			
Favored (%)	95.70	95.70	95.10
Allowed (%)	4.30	4.24	4.72
Disallowed (%)	0.00	0.06	0.17